Land subsidence modeling and mapping in Darab region, Iran

Advanced Tools for Studying Soil Erosion Processes

Loveimi, Mohammad Reza; Rezaei, Mahrooz; Mina, Monireh; Shafaie, Vahid; Kariminejad, Narges et al

https://doi.org/10.1016/B978-0-443-22262-7.00011-4

CHAPTER

16

Land subsidence modeling and mapping in Darab region, Iran

Mohammad Reza Loveimi[1], *Mahrooz Rezaei*[2,3], *Monireh Mina*[1], *Vahid Shafaie*[4], *Narges Kariminejad*[5] and *Michel J.P.M. Riksen*[3]

[1]Department of Soil Science, School of Agriculture, Shiraz University, Shiraz, Iran; [2]Meteorology and Air Quality Group, Wageningen University & Research, Wageningen, the Netherlands; [3]Soil Physics and Land Management Group, Wageningen University & Research, Wageningen, the Netherlands; [4]Department of Structural and Geotechnical Engineering, Széchenyi István University, Győr, Hungary; [5]Department of Natural Resources and Environmental Engineering, College of Agriculture, Shiraz University, Shiraz, Iran

1. Introduction

Land subsidence is a globally prevalent morphological phenomenon prevalent worldwide (Chitsazan et al., 2022). In general, land subsidence may cause a reduction in the Earth's land surface due to natural or human-induced activities, with the mobilization of solid or fluid underground materials being the primary cause (Herrera-García et al., 2021). Land subsidence and human activities have always been intertwined throughout history (Rahmati et al., 2019). Recently, over 150 major countries, including Mexico, Australia, Colombia, China, and the US, have reported land subsidence (Rahmani et al., 2022). It affects many global regions (Bhattarai et al., 2017; Mohammady et al., 2019) and can arise from various natural or anthropogenic factors, notably from groundwater extraction (Deng et al., 2017). Excessive groundwater extraction can result from various natural or human-induced activities including mining, mineral dissolution (Pacheco et al., 2006), and agriculture. In Iran, the agricultural sector is the predominant consumer of water resources. Numerous reports have highlighted that groundwater resources in vast areas of

Advanced Tools for Studying Soil Erosion Processes
https://doi.org/10.1016/B978-0-443-22262-7.00011-4

central Iran and the east and south of Iran serve as the sole source of water for agricultural, drinking, and industrial purposes. Iran comprises six major watersheds and 609 plains, with approximately 267 being water deficient. Given the vital role of water in human life and agriculture, many of these plains have been depleted (Najafi et al., 2020). Overextraction and aquifer depletion can result in land subsidence, manifesting abruptly or gradually due to a mix of natural and anthropogenic factors (Zhang et al., 2023; Gharechaee et al., 2023). The consequences of land subsidence include significant damage to infrastructure, such as buildings, transport networks, drainage systems, and underground pipelines (Cigna and Tapete, 2021). Beyond environmental changes, land subsidence affects socioeconomic activities. In addition to these direct effects, several indirect results have been obtained, such as reduced groundwater storage capacity, water contamination, and heightened flood hazards (Nhu et al., 2020). Safeguarding fertile agricultural land and infrastructure from subsidence necessitates the optimization of land subsidence mapping, thus enabling land-use planners to manage resources in a sustainable manner (Mohammady et al., 2019).

Different methods are generally employed worldwide to assess the zone subsidence susceptibility. For instance, data mining methods and machine learning models have proven to be effective in conducting essential studies to optimally control land subsidence and mitigate its potential risks (Rahmati et al., 2019). Machine learning algorithms are among the best approaches for prioritizing and determining the significance of factors affecting land subsidence performance (Eghrari et al., 2023). Machine learning has a significant advantage over traditional statistics-based approaches, particularly in earth sciences and ecology, because it can handle complex, high-dimensional datasets, including intricate interactions and missing values (Chitsazan et al., 2022). Many researchers have leveraged GIS-based machine learning algorithms across diverse Earth science and hydrology domains, such as groundwater mapping (Naghibi et al., 2016; Kariminejad et al., 2019; Arabameri et al., 2021; Gharechaee et al., 2023).

Given the significance of the Darab region in Fars Province as a key site susceptible to land subsidence, the objectives of the present study are (1) spatial modeling of land subsidence in the Darab plain of Fars Province; (2) evaluating different machine learning models both individually and collectively for spatial modeling of land subsidence; and (3) identifying the pivotal factors contributing to land subsidence in the area under study.

2. Material and methods

2.1 Study area

The Darab plain, situated in the southern province of Fars near the city of Darab, spans 54° 51′ 34″ to 54° 15′ 3″ east and latitude 28° 34′ 14″ to 28° 44′ 15″ N (Fig. 16.1). Darab is approximately 240 km away from Shiraz. Covering an area of approximately 7500 km^2, the region's average elevation is 1180 m above sea level. Darab has a predominantly temperate and warm climate, with most of the precipitation occurring as rainfall. According to the Meteorological Organization of Fars Province (2020), the annual rainfall seldom surpasses 350 mm, and the average annual temperature is 20.6°C.

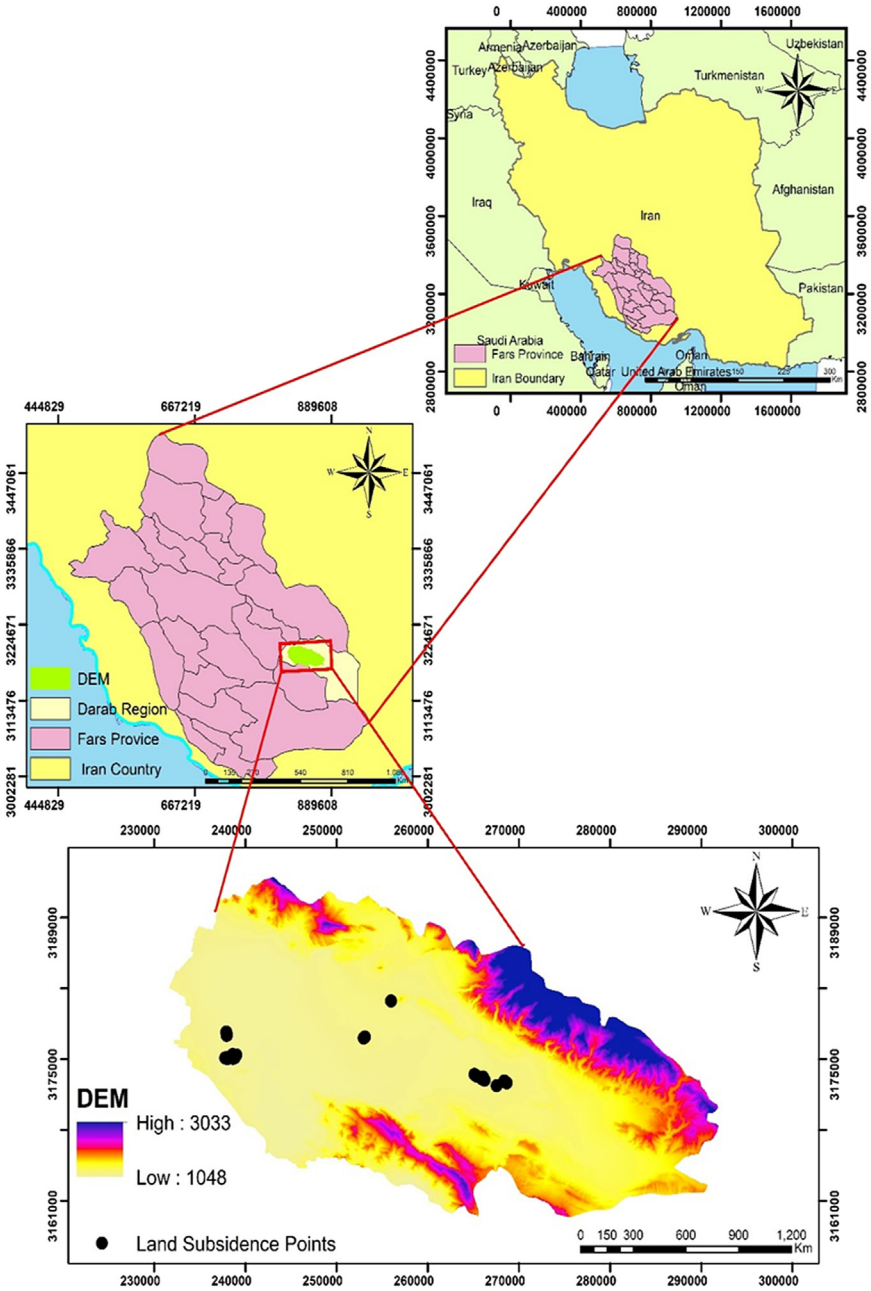

FIGURE 16.1 The geographical location of Fars province and the study area in Iran. *Black* dots indicate the location of land subsidence points.

2.2 Field work and soil analysis

In this study, our objective was to delineate land subsidence susceptibility using three individual models: maximum entropy (MaxEnt), support vector machine (SVM), artificial neural network (ANN), and a hybrid of these models. Land subsidence identification began with comprehensive field surveys, complemented by Google Earth imagery. In total, 114 subsidence points were documented using the Global Positioning System (GPS), and their inventory map was crafted using ArcGIS 10.5 software. Representative images of the subsidence within the study area are shown in Fig. 16.3. For each subsidence site, a set of physical soil attributes was examined. These attributes include soil roughness (Kuipers, 1957), compressive and shear strength (Rezaei et al., 2022), and morphological characteristics of the subsidence, namely its length, width, and height (Table 16.1).

Given the intricate nature of land subsidence, many factors can influence its control. In this context, the present study examined several soil and topography determinants. These included slope degree, slope aspect, distance to rivers, stream density, elevation, land use, normalized difference vegetation index (NDVI), plan curvature, profile curvature, topographic wetness index (TWI), pH, electrical conductivity (EC), mean annual rainfall, mean weight diameter (MWD), clay, silt, calcium carbonate equivalent (CCE), sodium content (Na), and organic matter (OM). Collectively, these elements provide insights into the prevailing conditions in the region, facilitating the assessment of the sensitivity and determination of land subsidence intensity. A flowchart detailing the various stages of our research is depicted in Fig. 16.2, and Fig. 16.3 shows instances of land subsidence observed in the study area.

2.3 Factors affecting land subsidence

Land subsidence is influenced by a combination of climatic-, topographic-, and soil-related factors. Consequently, a variety of such factors were integrated as inputs in our modeling efforts. These determinants encompass the prevailing conditions in the region and define their susceptibility to land subsidence. Maps representing all factors were generated using ArcMap and SAGA-GIS. Following the acquisition of the digital elevation model (DEM) map for the study area (at a scale of 1:25,000) from the Department of Natural Resources of Fars Province, primary topographic variables (such as elevation, slope degree, and aspect) and secondary variables (including the TWI and plan curvature) were extracted from the DEMs. Maps

TABLE 16.1 Results of land subsidence field studies.

N.	Length (m)	Width (m)	Depth (m)	Compressive strength (kg cm^{-2})	Shear strength (kg cm^{-2})	Soil roughness	Soil hydrophobicity (s)
Max	147.0	20.60	2.00	5.0	4.83	0.04	2.3
Ave	63.0	0.75	0.75	4.5	3.16	0.24	1.2
Min	0.5	0.12	0.15	3.0	1.50	0.01	<1

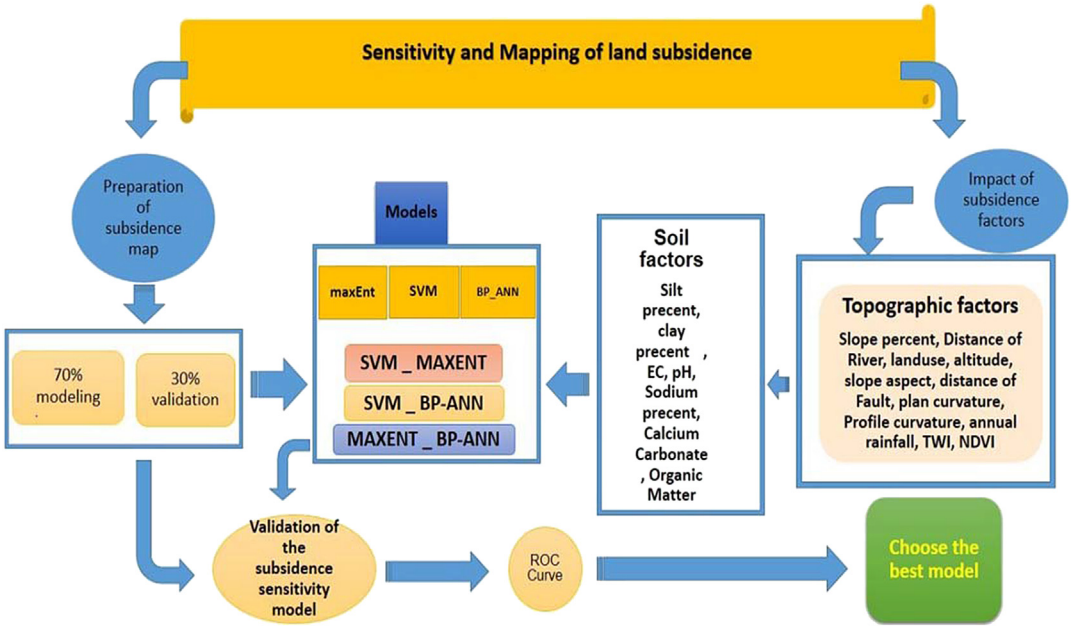

FIGURE 16.2 Flowchart of modeling steps of land subsidence in the study area.

FIGURE 16.3 Examples of land subsidence in the study area.

indicating the distance to rivers and stream density were crafted as information layers using ArcGIS software. The slope map of the study area was categorized into four classes using the natural breaks method, whereas the aspect map was divided into five directions: north, south, west, east, and flat. Similarly, the elevation map was segmented into four classes using the natural-break method. TWI is a secondary topographic variable that quantifies the rate of water accumulation at a specific location, as described by Eq. (16.1):

$$\mathrm{TWI} = \ln\left(\frac{\mathrm{A}}{\tan \mathrm{B}}\right) \tag{16.1}$$

where A represents the catchment area and B is the slope of the study area. The TWI for our study area was derived from the DEM of the area in SAGA-GIS.

Plan and profile curvatures describe the curvature of a slope that forms from the intersection of a horizontal plane with the ground surface. The Euclidean distance tool within the ArcGIS software was employed to determine the distance to the river. The distance map was subsequently divided into four classes using the natural break method. A stream density map of the study area was created using the ArcGIS linear compaction tool.

The NDVI represents the vegetation cover of the study area. As such, it can both directly and indirectly illustrate hydrological, and occasionally lithological, characteristics. This index was employed to quantitatively assess the relationship between land subsidence and the NDVI. The NDVI map for the region was derived from the average values from 2016 to 2020. NDVI was calculated and plotted using the following formula (Eq. 16.2):

$$\mathrm{NDVI} = \frac{\mathrm{band5} - \mathrm{band4}}{\mathrm{band5} + \mathrm{band4}} \tag{16.2}$$

Bands 4 and 5 represent the infrared and near-infrared wavelengths, respectively. The factors incorporated in this study are shown in Fig. 16.4.

2.4 Inverse distance weighted method

All interpolation techniques operate based on the foundational assumption that points in closer proximity exhibit greater correlation and similarity than those situated further apart. The IDW method hinges on the premise that the correlation and similarity between neighboring points are inversely proportional to the distance between them (Mohammed et al., 2022). In this study, the IDW statistical method was used to estimate the factors that influence land subsidence. Within the IDW framework, the influence of the studied variable diminishes as distance increases. Thus, at unmeasured locations, the continuous variable closely resembled its value at the nearest sampled points. Distance serves as a variable weight when predicting values at unmeasured locations (Kariminezhad, 2019).

In our approach to generating soil maps using the GS+ software, a spatial correlation was determined among the attributes at the sampled locations. Initially, the semivariability for each attribute was discerned and the potential anisotropy in the spatial continuity of the

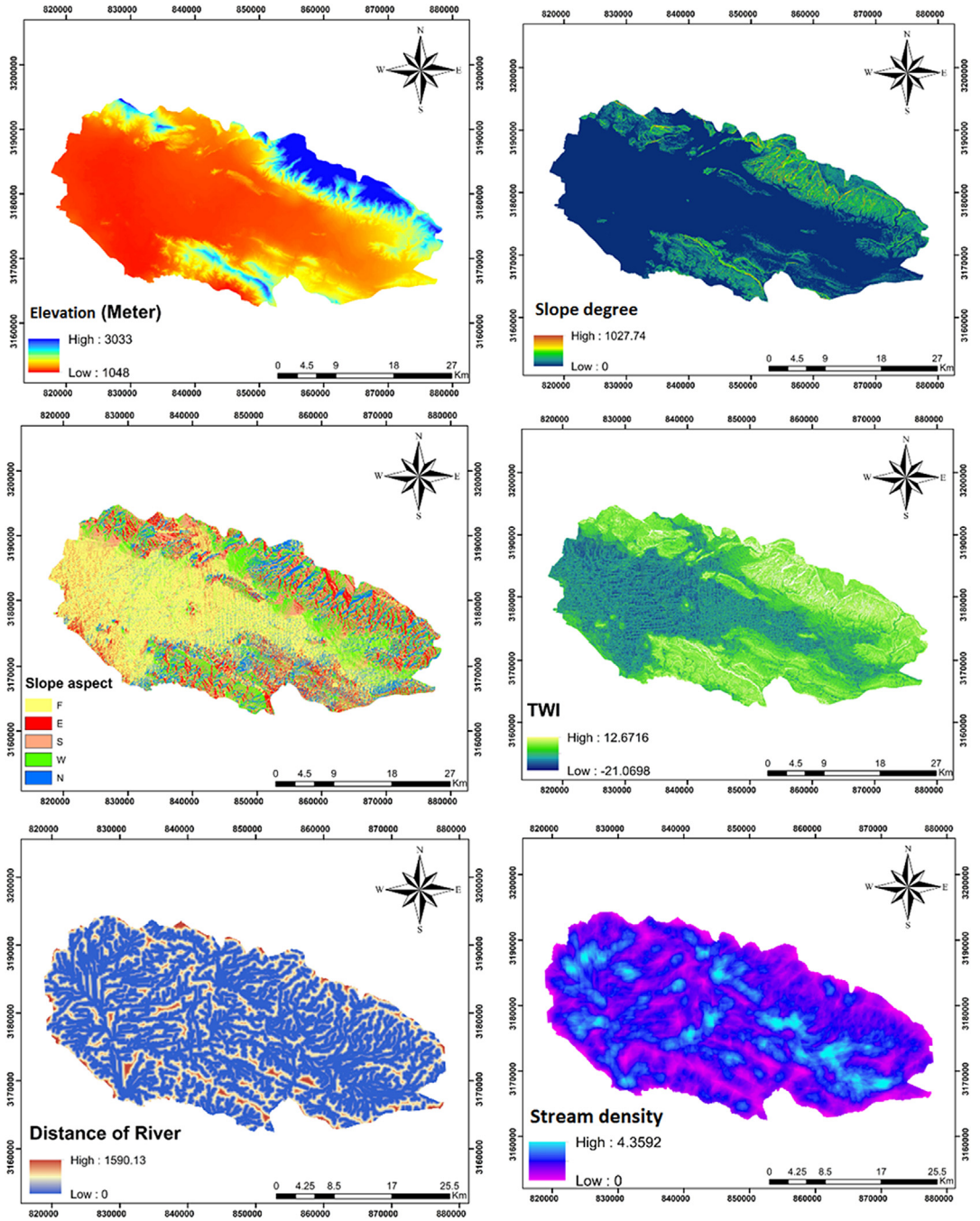

FIGURE 16.4 Land subsidence conditioning factors. Elevation, slope degree, slope aspect, topographic wetness index (TWI), distance of rivers, stream density, land use, normalized difference vegetation index (NDVI), plan curvature, profile curvature, clay, silt, pH, electrical conductivity (EC), mean weight diameter (MWD), organic matter (OM), sodium content (Na), calcium carbonate equivalent (CCE), and mean annual rainfall.

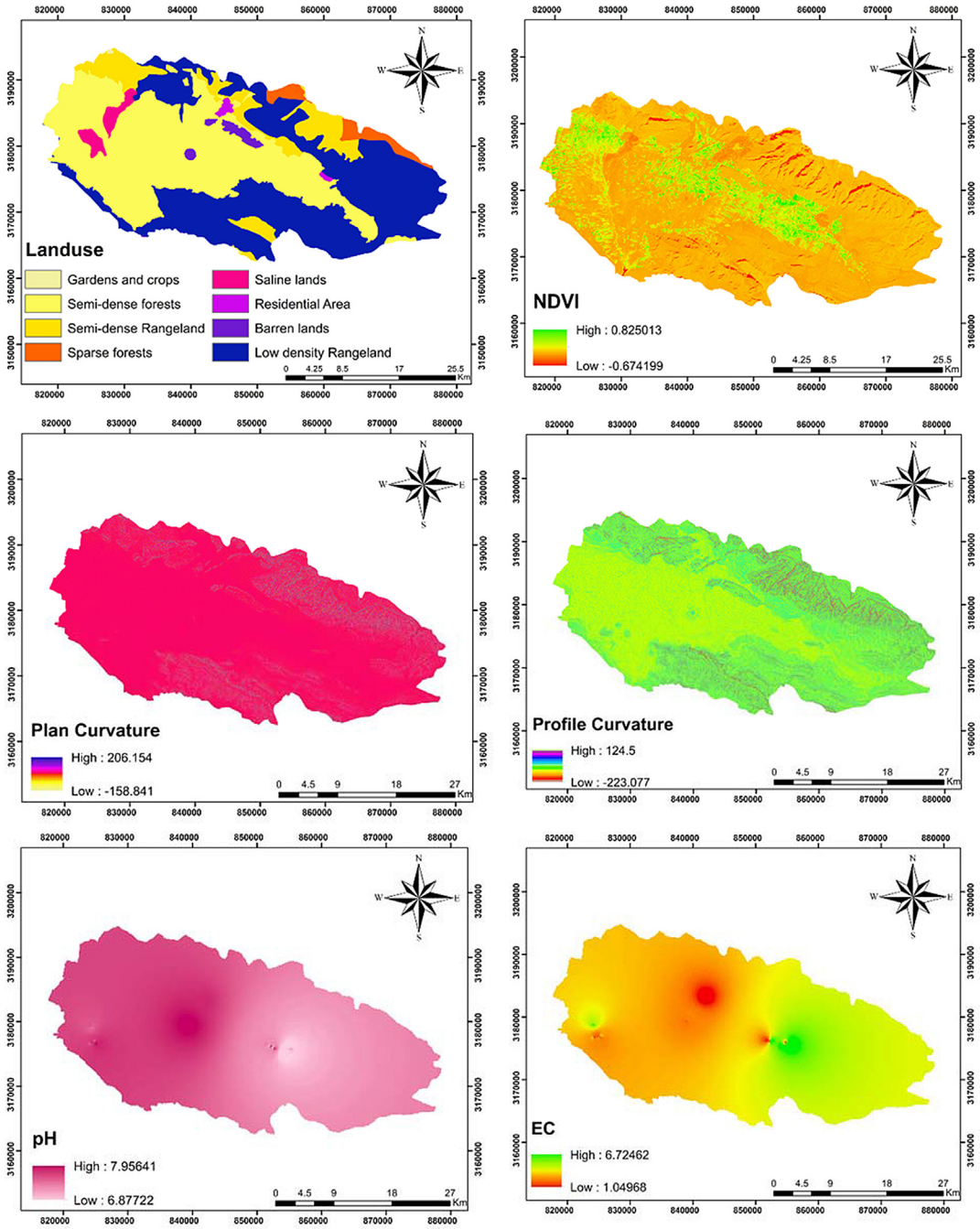

FIGURE 16.4 cont'd

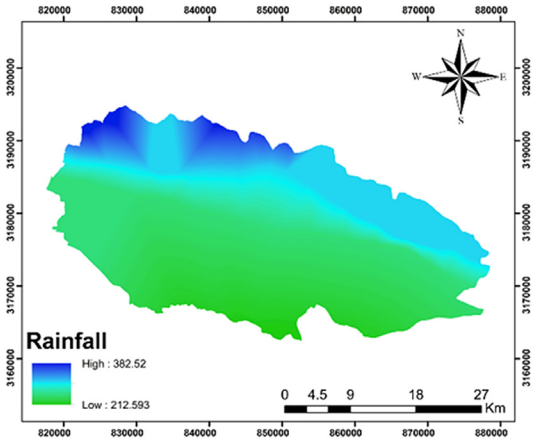

FIGURE 16.4 cont'd

data was explored. Subsequently, each attribute was calculated using semiexperimental variance, as shown in Eq. (16.3).

$$y(h) = \frac{1}{2N(h)} \sum_{i=1}^{n(h)} \{z(xi) - z(xi+h)\}^2 \tag{16.3}$$

Here:

- $y(h)$ represents the experimental semivariance for all pairs within a lag distance h;
- $N(h)$ denotes the number of point pairs separated by distance h (i.e., $(xi, xi + h)$);
- $z(xi)$ is the value of the variable at the sample location xi;
- $z(xi + h)$ indicates the variable's value at the sample location $xi + h$.

2.5 Collinear investigation of independent processes on land subsidence

Upon finalizing the factors influencing land subsidence and before embarking on the modeling process, it becomes essential to examine the collinearity among these independent factors. This examination ensures the removal of interdependent factors from the model and minimizes potential errors in the model's results. Multicollinearity analysis is a crucial method for selecting the significant factors. This method focuses on filtering out the causative factors of land subsidence that are highly correlated because such correlations might produce inaccurate outputs and uncertain predictions.

Our study probed multicollinearity through tolerance (TOL) and variance inflation factor (VIF) values associated with land subsidence factors. Indicators of multicollinearity problems occur when the TOL value drops below 0.1 or when the VIF surpasses 5 (Mina et al., 2022). To delve deeper into the linearity of these factors, both the VIF and TOL metrics were employed using SPSS software (Garosi et al., 2019).

2.6 Predictive models

2.6.1 Maximum entropy (MaxEnt)

The MaxEnt algorithm operates on the maximum entropy principle and is one of the foremost predictive machine-learning models used today. Fundamentally, MaxEnt estimates the probability distribution of a target event based on the maximum-entropy principle. In this study, the probability distribution of land subsidence occurrences was estimated. Given a probabilistic dataset, MaxEnt invariably selects a distribution with the highest entropy.

Phillips' laid out the foundational principles of MaxEnt modeling, which were primarily tailored for ecological modeling and the assessment of species distribution (Kariminejad et al., 2019). MaxEnt belongs to the machine-learning model family. Distinctively, this model, unlike many of its counterparts, is geared toward performing modeling based solely on occurrence points. This method involves identifying prevalent and uniformly distributed variables across a region to ascertain an unidentified distribution. Initially, the model scrutinizes and evaluates the layers associated with environmental variables on species distribution, leveraging training data pertinent to the study region. Subsequently, it assesses the likelihood of the occurrence of a particular species across the entire area (Mohammady et al., 2019).

2.6.2 Support vector machine

SVM is a supervised machine-learning technique extensively employed for statistical tasks, notably categorization and regression analysis. One of its salient advantages is its ability to minimize complexity, making it adept at both classification and regression challenges (Pourghasemi et al., 2020).

SVM's operational principle of SVM revolves around data classification. Within this classification paradigm, the objective is to select a linear delineation that provides the most reliable margin between the data classes (Abdollahi et al., 2019). Particularly in nonlinear scenarios, SVM proves invaluable for predicting phenomena such as land subsidence. This model employs foundational functions, such as sigmoid, polynomial, linear, and radial functions. These functions influence the predictive accuracy of the SVM (Garosi et al., 2019).

The efficacy of SVM is significantly contingent on kernel choice. The radial basis function (RBF) kernel is favored among the available options. Typically, the RBF kernel outperforms linear, sigmoid, and polynomial kernels, and is often the best choice because of its robustness and fewer numerical challenges (Abdollahi et al., 2019).

2.6.3 Artificial neural network

The ANN is one of the most precise and ubiquitously applied forecasting models. Its versatility has been demonstrated across a multitude of domains, ranging from socioeconomic forecasting to stock analysis and natural hazard susceptibility mapping. At its core, ANN is a dynamic statistical framework tailored to discern nonlinear correlations between the input and output variables within a dataset.

Analogous to human neural networks, ANNs encompass algorithms adept at analyzing and predicting the nonlinear attributes of phenomena. Among the spectrum of algorithms

integral to the ANN model, multilayer perceptron (MLP) is the most popular and has been consistently chosen by numerous researchers. Within the MLP, nodes in the hidden layers shoulder the responsibility of data analysis. The input layers encapsulate the factors influencing land subsidence, whereas the output layer is used to generate a subsidence susceptibility map. The hidden and output layers harness data from the input nodes and process them to facilitate accurate model predictions (Pourghasemi et al., 2017). As elucidated by Mandal and Mandal (2018), the MLP-driven ANN model seamlessly integrates three layers: input, hidden, and output layers.

2.6.4 *Hybrid models*

Hybrid models combine the results of individual models to create a unified, continuous model, aiming to bolster predictive accuracy. This methodology has increasingly piqued the interest of model developers, particularly those entrenched in data-mining pursuits. Most hybrid techniques adopt weighted integrals from stand-alone models to optimize the results.

This study introduced an integration technique termed "heterogeneous classification." This method formulates sophisticated equations using foundational arithmetic operations such as multiplication, division, addition, and subtraction. Upon implementing the three weighted average models, Eq. (16.4) was deployed to establish the hybrid models:

$$\mathrm{EM} = \frac{\sum_{i=0}^{n} (\mathrm{AUSRC}i * Mi)}{\sum_{i=0}^{n} \mathrm{AUSRC}} \tag{16.4}$$

Here, EM signifies the output of the hybrid models, whereas AUSRCi represents the AUSRC value derived from the individual model Mi. The efficacy of such models, particularly in terms of their adaptability and precision, is a testament to their design (Pourghasemi et al., 2017).

2.7 Model evaluation

To model the land subsidence susceptibility maps in this study, 70% of the land subsidence points were employed for individual and combined modeling using the ModEco software (Abdollahi et al., 2019). The remaining 30% of the points were used for the model evaluation and validation.

The ROC and AUC were employed for statistical analyses, which researchers have extensively adopted to validate various natural hazard maps (Zhang and Wang, 2019). Model accuracy was assessed using the ROC curve, with AUC as an indicator of a model's validity and proficiency in distinguishing between the occurrence and nonoccurrence of subsidence events.

Typically, the AUC values range from 0.5 1. A value of 1 signifies an ideal modeling outcome, whereas a value close to 0.5 suggests an ineffective model. The interpretation of the AUC values is as follows (Abdollahi et al., 2019):

TABLE 16.2 Physical and chemical laboratory results of Darab region, Fars Province.

Parameters	Unit	MAX	Mean	MIN	SD
pH	–	7.96	7.61	6.87	0.27
EC	ds m^{-1}	7.59	2.59	0.79	1.80
Na^+	%	85.63	54.54	29.24	18.17
OM	%	0.99	0.62	0.14	0.22
MWD	mm	0.90	0.57	0.33	0.12
Silt	%	64.41	44.95	26	9.52
Clay	%	23.64	14.83	7.28	3.73
CCE	%	65.25	50.24	37.75	6.20

CCE, calcium carbonate equivalent; *EC*, electrical conductivity; *MWD*, aggregate mean weight diameter; *Na*, soil sodium content; *OM*, organic matter; *pH*, soil acidity.

- 0.5–0.6: Weak
- 0.6–0.7: Moderate
- 0.7–0.8: Good
- 0.8–0.9: Very good
- 0.9–1.0: Excellent

3. Results and discussion

3.1 Effective laboratory factors

Table 16.2 presents the statistical summary of the measured properties. The normality of the data distribution was assessed using the Kolmogorov–Smirnov test in the SPSS software. Any nonnormal data distribution was transformed into a normal distribution using suitable conversions.

The pH values suggest that the soil in the study area had a neutral disposition. The EC values indicate a moderate level of soil salinity. The OM content indicated that the region had a relatively low concentration of OM. Based on the soil texture tests, the texture of the study area is predominantly loam to silty loam. The high mean CCE of 50.24% suggests a predominantly limestone composition in the area. Furthermore, the average sodium (Na^+) content of 54.54% was significantly higher than that of the standard classifications.

3.2 Geostatistical interpolation methods

Table 16.3 provides the coefficients of the best-fit model corresponding to the semivariance of the investigated soil characteristics. Geostatistical analysis results indicated that the exponential model was the best fitting semivariogram model for all the evaluated factors. Moreover, for all factors, excluding Na^+ and CCE, the spatial class was determined to be moderate.

TABLE 16.3 Models and parameters of semivariogram.

Parameters	Unit	Model	Nugget (C0)	Sill (C0 + C)	C0/(C0 + C)	Spatial class	R^2	RSS
pH	–	Exponential	0.04	0.90	0.50	Moderate	0.90	0.01
EC	ds m^{-1}	Exponential	0.29	0.01	0.65	Moderate	0.42	0.07
Na	%	Exponential	0.05	0.80	0.93	Low	0.51	0.04
OM	%	Exponential	0.02	0.06	0.65	Moderate	0.74	0.01
MWD	mm	Exponential	0.03	0.06	0.50	Moderate	0.71	0.01
Silt	%	Exponential	0.03	0.13	0.76	Moderate	0.72	0.01
Clay	%	Exponential	0.07	0.16	0.54	Moderate	0.75	0.01
CCE	%	Exponential	0.01	0.26	0.94	Low	0.52	0.01

CCE, calcium *carbonate* equivalent; *EC*, electrical conductivity; *MWD*, aggregate mean weight diameter; *Na*, soil sodium content; *OM*, organic matter; *pH*, soil acidity.

3.3 Collinearity analysis of effective factors in land subsidence

Table 16.4 presents the collinearity analysis results for the 19 considered factors. A TOL value of 0.1 and a VIF value exceeding 10% suggest potential multicollinearity issues between the variables (Garosi et al., 2019). Notably, a higher VIF value corresponds to a lower TOL

TABLE 16.4 Multicollinearity test among land subsidence conditioning factors.

	Collinearity statistics			Collinearity statistics	
Factors	**VIF (%)**	**TOL**	**Factors**	**VIF (%)**	**TOL**
Elevation	1.97	0.50	Clay	2.79	0.42
Slope degree	1.70	0.58	Silt	1.82	0.54
Slope aspect	1.39	0.71	PH	2.15	0.46
Distance to rivers	1.39	0.71	OM	1.48	0.67
Profile curvature	1.33	0.75	Na^{+1}	2.59	0.38
Land use	2.69	0.39	EC	2.61	0.38
Stream density	1.61	0.62	MWD	1.14	0.87
Plan curvature	1.58	0.63	NDVI	1.34	0.74
Annual rainfall	2.01	0.49	TWI	2.33	0.42
CCE	2.75	0.40			

CCE, calcium carbonate equivalent; *EC*, electrical conductivity; *MWD*, aggregate mean weight diameter; *Na*, sodium; *NDVI*, normalized difference vegetation index; *OM*, organic matter; *TOL*, tolerance; TWI, topographic wetness index; *VIF*, variance inflation.

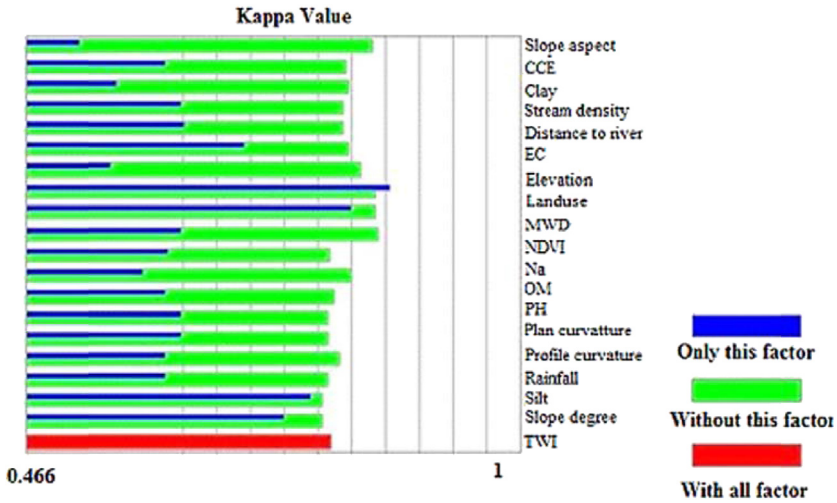

FIGURE 16.5 Prioritization of factors affecting land subsidence using the RBF method based on the SVM model.

value. Our results indicated the absence of any significant multicollinearity problems among the evaluated factors.

3.4 Prioritization of factors affecting land subsidence

Fig. 16.5 depicts the prioritization of factors impacting land subsidence, which was performed using the RBF method within the SVM model. The analysis, encompassing topographic, soil (laboratory), hydrological, and environmental factors in the Darab region, highlighted elevation and land use as the principal contributors to subsidence. Zhang et al. (2023) also indicated that land use and related land management practices could be linked to land subsidence. They found that land management, specifically focusing on water and soil conservation, could mitigate land subsidence complications. Neglecting these principles can intensify the onset and spread of subsidence (Chaussard et al., 2014). Abdollahi et al. (2019) found that changes in land use, largely attributed to human activities, are primary catalysts for land collapse.

Other influential factors included slope degree, TWI, distance to rivers, stream density, NDVI, plan curvature, profile curvature, Na^+, rainfall, CCE, pH, OM, and silt. Other notable factors included clay, EC, slope aspect, and MWD. The significance assigned to elevation and land use aligns with previous studies, corroborating the findings of this study (Rahmati et al., 2019; Chitsazan et al., 2022; Eghrari et al., 2023; Zhang et al., 2023; Gharechaee et al., 2023).

3.5 Land subsidence susceptibility mapping

Susceptibility maps for land subsidence derived using the ANN, MaxEnt, and SVM models are presented in Fig. 16.6. In addition, hybrid models have been visualized, encompassing combinations such as SVM-MaxEnt, SVM-ANN, and ANN-MaxEnt. Susceptibility

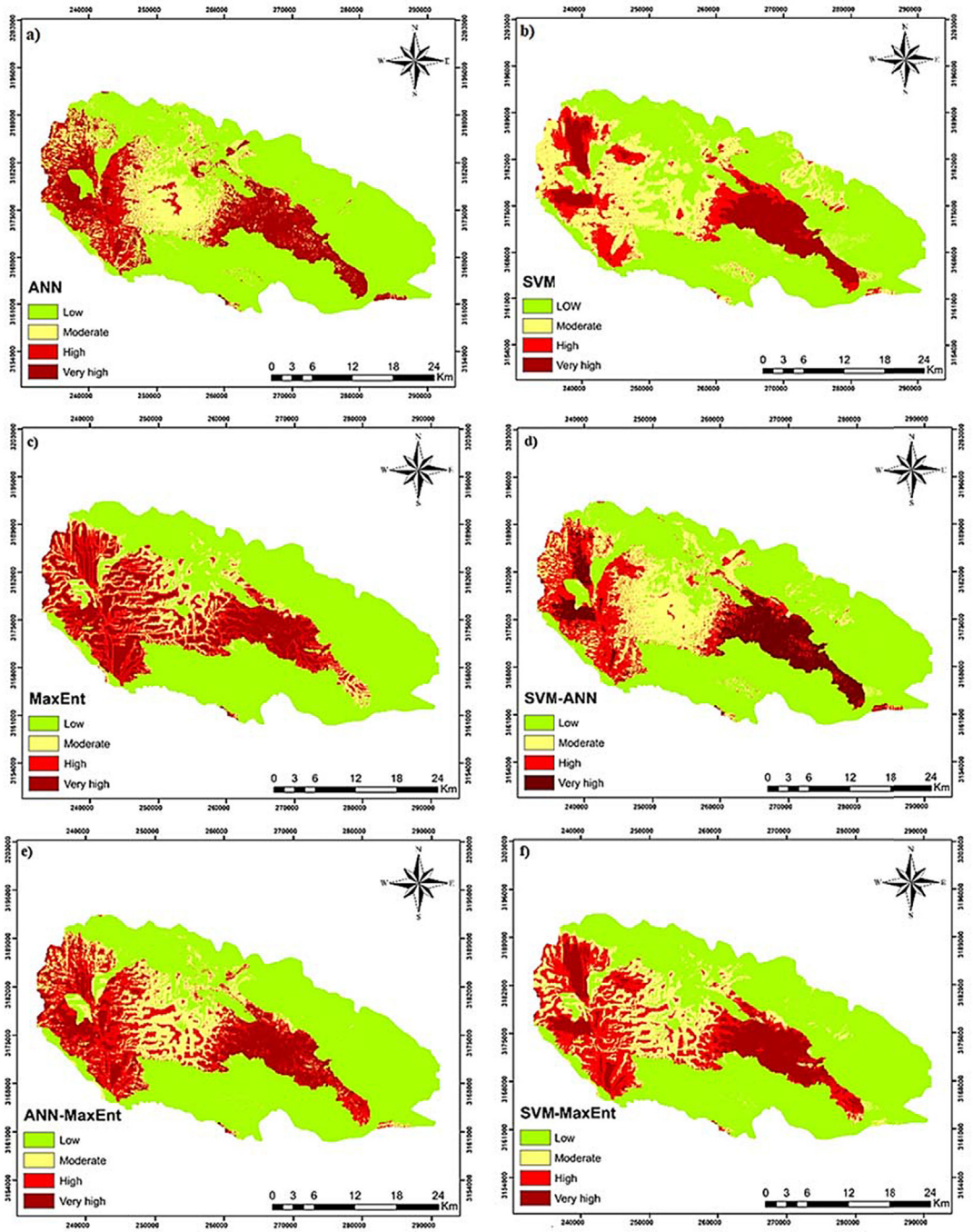

FIGURE 16.6 Land subsidence susceptibility mapping. (a) ANN, (b) SVM, (c) MaxEnt, (d) SVM-ANN, (e) ANN-MaxEnt, (f) SVM-MaxEnt.

TABLE 16.5 Percentage of each susceptibility class in the final land subsidence using different models.

Susceptibility class	ANN	MaxEnt	SVM	ANN-MaxEnt	SVM-ANN	SVM-MaxEnt
Low	58.77	58.94	56.22	57.97	57.37	58.12
Moderate	16.47	10.67	23.15	16.47	17.71	14.92
High	11.10	15.32	10.15	11.02	13.58	16.17
Very high	13.64	15.04	10.47	13.61	11.32	10.77

maps, segmented using the natural break method, were categorized into four distinct levels: low, moderate, high, and very high. A comprehensive breakdown of the percentage representation of each category in the final subsidence maps is presented in Table 16.5.

The land subsidence modeling results indicated varying susceptibilities across the different models. The percentage distribution across susceptibility classes offers insights into the performance of susceptibility maps. Modeling and simulation systems serve as crucial instruments for decision-making, broadening the understanding of environmental hazards. The diverse structures of these modeling approaches often yield varied results and performances in terms of spatial predictions. Such variations underline the importance of understanding the implications of these models in environmental studies, particularly as they guide decisions made by environmental planners and managers (Rahmati et al., 2019). A myriad of available modeling approaches equips decision-makers with tools to conceptualize and implement eco-conscious initiatives (Chitsazan et al., 2022). Intriguingly, even when consistent modeling techniques are employed across different scenarios, disparities in predictions and methodologies can emerge. Hence, there is an imperative need for comparative studies to juxtapose the efficacy of models under identical conditions to provide an impartial evaluation of their capabilities. Furthermore, it is pivotal that such results are interpreted in tandem with the AUC values for a comprehensive understanding (Abdollahi et al., 2019).

3.6 Evaluation of land subsidence susceptibility maps

The evaluation results for the land subsidence susceptibility maps generated using individual ANN, MaxEnt, and SVM models, as well as the combined ANN-MaxEnt, SVM-ANN, and SVM-MaxEnt models, are detailed in Fig. 16.7 and Table 16.6. Land subsidence locations (30%) that were not used during the modeling were applied to evaluate the models using the ROC curve. Overall, these evaluations highlight a remarkable consistency in the spatial modeling accuracy of the land subsidence maps across the models, with AUC values ranging from 0.89 to 0.92. Despite this overarching consistency, minor variations were noted across the susceptibility classifications of different models. Such discrepancies may be attributed to the intrinsic modeling processes of each technique. Notably, the MaxEnt model exhibited an accuracy metric of 0.92. This suggests its superior efficacy, corroborated by various studies in which the MaxEnt model has consistently demonstrated high performance in different modeling scenarios. A pivotal metric for discerning the best model for predicting

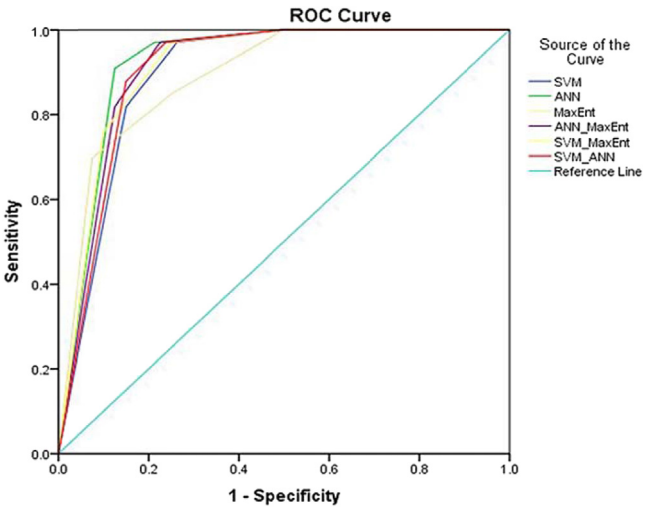

FIGURE 16.7 ROC curve for different models based of 30% of land subsidence points.

TABLE 16.6 Results of evaluation of land subsidence susceptibility maps using different models.

Area under the curve (AUC)					
				Asymptotic 95% confidence interval	
Models	Area	Standard error	Asymptotic significant	Lower bound	Upper bound
ANN	0.90	0.02	0	0.85	0.96
ANN-MaxEnt	0.91	0.02	0	0.86	0.96
MaxEnt	0.92	0.02	0	0.87	0.97
SVM	0.89	0.02	0	0.83	0.95
SVM-ANN	0.91	0.02	0	0.85	0.96
SVM-MaxEnt	0.89	0.03	0	0.83	0.95

land subsidence events is the elevated value of the models' receiver operating characteristic and area under curves. Essentially, the higher these values, the more precise and reliable the model is deemed (Mohammady et al., 2019).

Among the evaluated methods, MaxEnt demonstrated superior performance in identifying areas that are vulnerable to subsidence. Given the adaptability of the proposed method to diverse regions worldwide, the application of the MaxEnt model is strongly recommended. In this study, elevation emerged as the primary factor exacerbating land subsidence. Other important factors included slope degree, TWI, distance to rivers, and stream density. A significant limitation of this study was the absence of subsidence rate and water table data for

the region. This lack of data means that we could not analyze the incremental effects of various factors on subsidence over time and the role of the groundwater level on subsidence. Therefore, future research should consider utilizing subsidence rates and the water table as pivotal variables in land subsidence susceptibility modeling, provided that such data become available.

4. Conclusion

The main aim of this study was to map the risk of land subsidence in the Darab region of the Fars Province and identify the most important factors involved in using machine learning algorithms. Susceptibility maps for land subsidence were generated by leveraging the correlation between 114 subsidence locations and 19 different climatic, soil, and topographical factors.

Of the 19 factors examined for their influence on land subsidence, elevation and land use emerged as the most influential in the region. Broadly, these findings underscore the capability of machine learning algorithms in precision-predicting areas susceptible to land subsidence.

Land subsidence is multifaceted, and initiating protective watershed management interventions to curtail its spread is imperative. Field surveys and local interviews revealed that the majority of subsidence incidents occurred in agricultural land. Mismanagement of soil and overextraction of groundwater have precipitated the deterioration of agricultural lands, leading to significant degradation.

Given these findings, it is pivotal to regulate the number of piezometric wells in the region, relocate residential zones from high-risk areas to safer ones, and promote the cultivation of low-water-demand crops to mitigate and prevent further land subsidence.

Further research could develop a comprehensive risk assessment framework by incorporating vulnerability facets, such as potential assets and populations susceptible to land subsidence. Although such endeavors would significantly bolster real-world applicability in land subsidence modeling, they require access to extensive, contextually relevant datasets, transcending the confines of the study region to achieve global relevance.

References

Abdollahi, S., Pourghasemi, H.R., Ghanbarian, G.A., Safaeian, R., 2019. Prioritization of effective factors in the occurrence of land subsidence and its susceptibility mapping using an SVM model and their different kernel functions. Bulletin of Engineering Geology and the Environment 78 (6), 4017–4034.

Arabameri, A., Yariyan, P., Santosh, M., 2021. Land Subsidence Spatial Modeling and Assessment of the Contribution of Geo-Environmental Factors to Land Subsidence: Comparison of Different Novel Ensemble Modeling Approaches.

Bhattarai, R., Alifu, H., Maitiniyazi, A., Kondoh, A., 2017. Detection of land subsidence in Kathmandu Valley, Nepal, using DInSAR technique. Land 6 (2), 39.

Chaussard, E., Wdowinski, S., Cabral-Cano, E., Amelung, F., 2014. Land subsidence in central Mexico detected by ALOS InSAR time-series. Remote Sensing of Environment 140, 94–106.

Chitsazan, M., Rahmani, G., Ghafoury, H., 2022. Land subsidence susceptibility mapping using PWRSTFAL framework and analytic hierarchy process: fuzzy method (case study: Damaneh-Daran Plain in the West of Isfahan Province, Iran). Environmental Monitoring and Assessment 194 (3), 192.

Cigna, F., Tapete, D., 2021. Present-day land subsidence rates, surface faulting hazard and risk in Mexico City with 2014–2020 Sentinel-1 IW InSAR. Remote Sensing of Environment 253, 112161.

Deng, Z., Ke, Y., Gong, H., Li, X., Li, Z., 2017. Land subsidence prediction in Beijing based on PS-InSAR technique and improved Grey-Markov model. GIScience and Remote Sensing 54 (6), 797–818.

Eghrari, Z., Delavar, M.R., Zare, M., Beitollahi, A., Nazari, B., 2023. Land subsidence susceptibility mapping using machine learning algorithms. ISPRS Annals of the Photogrammetry, Remote Sensing and Spatial Information Sciences 10, 129–136.

Garosi, Y., Sheklabadi, M., Conoscenti, C., Pourghasemi, H.R., Van Oost, K., 2019. Assessing the performance of GIS-based machine learning models with different accuracy measures for determining susceptibility to gully erosion. Science of the Total Environment 664, 1117–1132.

Gharechaee, H., Samani, A.N., Sigaroodi, S.K., Baloochiyan, A., Moosavi, M.S., Hubbart, J.A., Sadeghi, S.M.M., 2023. Land subsidence susceptibility mapping using Interferometric Synthetic Aperture Radar (InSAR) and machine learning models in a semiarid region of Iran. Land 12 (4), 843.

Herrera-García, G., Ezquerro, P., Tomás, R., Béjar-Pizarro, M., López-Vinielles, J., Rossi, M., Ye, S., 2021. Mapping the global threat of land subsidence. Science 371 (6524), 34–36.

Kariminejad, N., Hosseinalizadeh, M., Pourghasemi, H.R., Bernatek-Jakiel, A., Campetella, G., Ownegh, M., 2019. Evaluation of factors affecting gully headcut location using summary statistics and the maximum entropy model: Golestan Province, NE Iran. Science of the Total Environment 677, 281–298.

Kuipers, H., 1957. A reliefmeter for soil cultivation studies. Netherlands Journal of Agricultural Science 5 (4), 255–262.

Mandal, B., Mandal, S., 2018. Analytical hierarchy process (AHP) based landslide susceptibility mapping of Lish river basin of eastern Darjeeling Himalaya, India. Advances in Space Research 62 (11), 3114–3132.

Mina, M., Rezaei, M., Sameni, A., Ostovari, Y., Ritsema, C., 2022. Predicting wind erosion rate using portable wind tunnel combined with machine learning algorithms in calcareous soils, southern Iran. Journal of Environmental Management 304, 114171.

Mohammady, M., Pourghasemi, H.R., Amiri, M., 2019. Land subsidence susceptibility assessment using random forest machine learning algorithm. Environmental Earth Sciences 78, 1–12.

Mohammed, O.A., Vafaei, S., Kurdalivand, M.M., Rasooli, S., Yao, C., Hu, T., 2022. A comparative study of forest Fire mapping using GIS-based data mining approaches in western Iran. Sustainability 14 (20), 13625.

Naghibi, S.A., Pourghasemi, H.R., Dixon, B., 2016. GIS-based groundwater potential mapping using boosted regression tree, classification and regression tree, and random forest machine learning models in Iran. Environmental Monitoring and Assessment 188, 1–27.

Najafi, Z., Pourghasemi, H.R., Ghanbarian, G., Fallah Shamsi, S.R., 2020. Land-subsidence susceptibility zonation using remote sensing, GIS, and probability models in a Google Earth Engine platform. Environmental Earth Sciences 79, 1–16.

Nhu, V.H., Shirzadi, A., Shahabi, H., Singh, S.K., Al-Ansari, N., Clague, J.J., Ahmad, B.B., 2020. Shallow landslide susceptibility mapping: a comparison between logistic model tree, logistic regression, naïve Bayes tree, artificial neural network, and support vector machine algorithms. International Journal of Environmental Research and Public Health 17 (8), 2749.

Pacheco, J., Arzate, J., Rojas, E., Arroyo, M., Yutsis, V., Ochoa, G., 2006. Delimitation of ground failure zones due to land subsidence using gravity data and finite element modeling in the Querétaro valley, México. Engineering Geology 84 (3–4), 143–160.

Pourghasemi, H.R., Sadhasivam, N., Kariminejad, N., Collins, A., 2020. Gully erosion spatial modelling: role of machine learning algorithms in selection of the best controlling factors and modelling process. Geoscience Frontiers 11, 2207–2219.

Pourghasemi, H.R., Yousefi, S., Kornejady, A., Cerdà, A., 2017. Performance assessment of individual and ensemble data-mining techniques for gully erosion modeling. Science of the Total Environment 609, 764–775.

Rahmani, G., Chitsazan, M., Ghafouri, H., 2022. Predicting water level drawdown and assessment of land subsidence in Damaneh-Daran Aquifer by combining numerical and analytical models. Advanced Applied Geology 12 (2), 259–275.

Rahmati, O., Falah, F., Naghibi, S.A., Biggs, T., Soltani, M., Deo, R.C., Bui, D.T., 2019. Land subsidence modelling using tree-based machine learning algorithms. Science of the Total Environment 672, 239–252.

Rezaei, M., Mina, M., Ostovari, Y., Riksen, M.J., 2022. Determination of the threshold velocity of soil wind erosion using a wind tunnel and its prediction for calcareous soils of Iran. Land Degradation & Development 33 (13), 2340–2352.

Zhang, C., Wang, H., 2019. Robustness of the active rotary inertia driver system for structural swing vibration control subjected to multi-type hazard excitations. Applied Sciences 9 (20), 4391.

Zhang, L., Arabameri, A., Santosh, M., Pal, S.C., 2023. Land subsidence susceptibility mapping: comparative assessment of the efficacy of the five models. Environmental Science and Pollution Research 1–20.